AGU PUBLICATIONS

Geophysical Research Letters

RESEARCH LETTER
10.1002/2015GL065989

Key Points:
- Storm surge analyzed in integrated approach of in situ, satellite data, models
- SARAL reproduces surge height, underestimates high wave heights and wind speed
- A surge-induced subsidence of 4–6 cm is detected by GPS measurements.

Supporting Information:
- Movie S1
- Figure S1, Tables S1–S6, and Movie S1
- Text S1
- Figure S1

Correspondence to:
L. Fenoglio-Marc,
fenoglio@psg.tu-darmstadt.de

Citation:
Fenoglio-Marc, L., R. Scharroo, A. Annunziato, L. Mendoza, M. Becker, and J. Lillibridge (2015), Cyclone Xaver seen by geodetic observations, *Geophys. Res. Lett.*, *42*, 9925–9932, doi:10.1002/2015GL065989.

Received 2 SEP 2015
Accepted 12 OCT 2015
Accepted article online 15 OCT 2015
Published online 23 NOV 2015

Cyclone Xaver seen by geodetic observations

L. Fenoglio-Marc[1], R. Scharroo[2], A. Annunziato[3], L. Mendoza[1], M. Becker[1], and J. Lillibridge[4]

[1]Physical and Satellite Geodesy, Institute of Geodesy, Faculty of Civil and Environmental Engineering, Technische Universität Darmstadt, Darmstadt, Germany, [2]EUMETSAT, Darmstadt, Germany, [3]Joint Research Centre, European Commission, Ispra, Italy, [4]Laboratory for Satellite Altimetry, National Oceanic and Atmospheric Administration, College Park, Maryland, USA

Abstract Cyclone Xaver pounded the North Sea on 5–6 December 2013 and reached its maximum in the German Bight the second day. Combined geodetic measurements from the SARAL/AltiKa satellite and from a local geodetic network detect cross-shelf and alongshore variations and loading vertical deformation. The cross-shelf root-mean-square differences between observations and predictions are 30 cm for surge height, 2 m for significant wave height, and 4 m/s for wind speed, with significant biases. The different wind forcing mainly causes the predicted height differences. The smallest standard deviation difference between observed and predicted vertical displacements is from HyFlux2 forced by DWD wind, with a 52% reduction in the standard deviation by subtracting prediction from observations. The GPS network monitors the anticlockwise surge path with maximum land subsidence of 3–5 cm. The tide gauge network monitors both the anticlockwise path of the external wave and the surge associated with strong northwesterly winds.

1. Introduction

The North Sea region has a long history of extratropical cyclones representing a substantial hazard especially for the low-lying coastal areas along the Southern North Sea coasts [*Weisse and von Storch*, 2009; *Jensen and Mueller-Navarra*, 2008]. The associated extreme sea levels are caused by a combination of factors such as high astronomical tides, extreme wind-generated waves, and storm surges in response to fluctuations in local and remote winds and atmospheric pressure. In the German Bight the storm surges are associated with strong northwesterly winds over the entire North Sea and external waves triggered by low-pressure systems over the Northeast Atlantic [*Rossiter*, 1958].

The dynamical response of the coastal and shelf area (depths < 40 m) to a moving storm is complex. In deep water, the primary forcing is the atmospheric pressure deficit [*Mathers and Woodworth*, 2004]; near coast, the surface wind stress becomes increasingly important causing water piling up, with surges of up to 4 m [*Weisse et al.*, 2012; *Dangendorf et al.*, 2014].

Tide gauges continuously monitor variations of the storm surge near shore, while the altimeter satellites measure along the ground track offshore up to five 5 km from the coast, provided that overflight occurs at the right time. Valuable information on the spatial structure of a hurricane surge has been gained by combining altimetry and tide gauge measurements [*Scharroo et al.*, 2005; *Han et al.*, 2012; *Lillibridge et al.*, 2013]. Altimeter data are not yet included in operational storm surge forecasting, although they are used in the eSurge project of the European Space Agency (http://www.storm-surge.info).

The deformation of the Earth's crust in response to the nontidal sea level variations, called nontidal ocean loading (NTOL), has been analyzed from Global Positioning System (GPS) data, e.g., by *Williams and Penna* [2011] and *Zerbini et al.* [2004]. Storm surge loads have been detected in the North Sea by *Geng et al.* [2012], who studied large-scale coastal variations of nontidal loading observed by subdaily GPS and predicted by models.

In our study we focus on the largest storm surge signal captured by satellite altimetry to date, nearly 3 m, in order to analyze the capability of combining geodetic measurements to detect both alongshore and cross-shelf variations and land subsidence also at short spatial and temporal scales. The dense network includes satellite altimetry and in situ measurements of sea level heights from 13 tide gauge stations colocated with GPS receivers and other in situ stations providing wave and wind speed data. Methodology and data are presented in section 2. In section 3 surge and wave height, wind speed, and vertical displacement are assessed

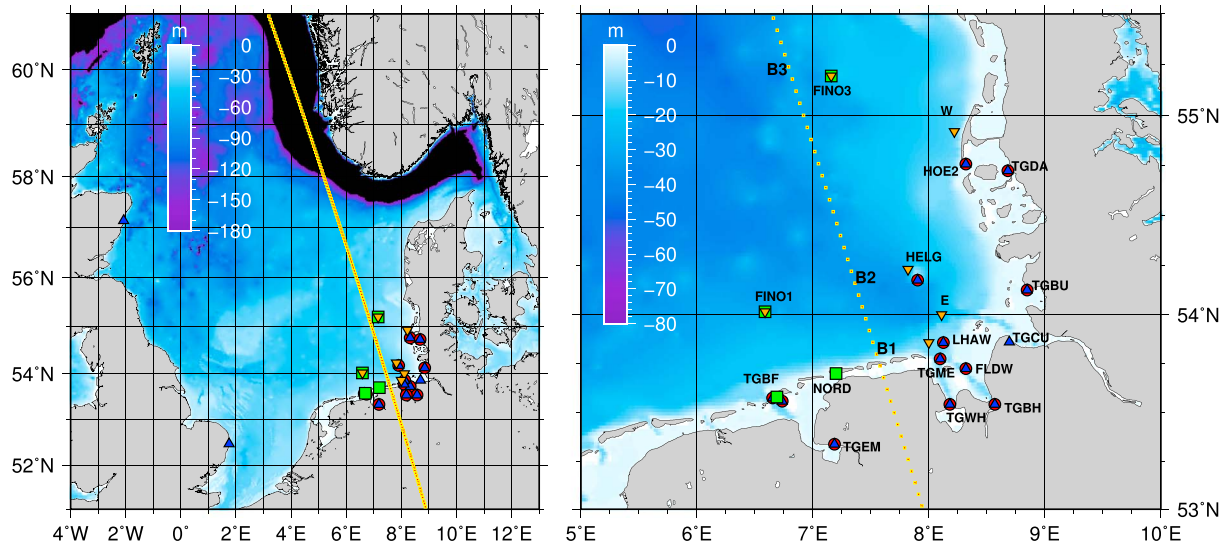

Figure 1. Study area: (right) German Bight and (left) enlarged to North Sea with the SARAL/AltiKa altimeter ground track and in situ stations with GPS (circle), sea level (triangle), wave height (inverted triangle), and wind speed (square) data. Bathymetry is shown.

from observations and models. As a spin-off, the departure of predicted and observed values enables us to assess the quality of the storm surge models themselves.

2. Methodology and Data

The Total Water Level Envelope (TWLE) has three components: ocean tide, storm surge, and wind wave setup. The wind wave setup, which is the increase in mean water level at the coast due to the presence of waves, is not contained in tide gauges measurements due to the measurement system, which filters waves out. Satellite altimetry also fails to observe to wave setup as it cannot measure close enough to the coast to properly sample the surf zone. Hence, in the following we ignore the component of wave setup in both tide gauge and altimeter measurements.

We analyze here the storm surge, which is the large-scale rise of the sea surface caused by high wind speed and low atmospheric pressure. First, we compute the storm surge height (SS) as the difference between the altimetric/tide gauge/model sea level and the ocean tide. Wave height (SWH) and wind speed (U10) are the two other surge parameters studied. Further on, we compute the vertical displacement of the Earth's crust due to the nontidal ocean loading NTOL. See Table S2 for the corrections applied.

2.1. Surge Height, Wind, and Waves

The SARAL/AltiKa satellite launched on 25 February 2013 carries a Ka band satellite radar altimeter. The altimeter data are from the Radar Altimeter Database System (RADS) [*Scharroo et al.*, 2013], with SWH and U10 values corresponding to the standard agency products. We compute the altimeter TWLE as the difference of orbital altitude and corrected radar range relative to the mean sea surface model DTU10 [*Andersen and Knudsen*, 2010]. Geophysical and media corrections for ionospheric and tropospheric path delay, sea state bias, solid Earth and load tide have been applied, while ocean tide and inverse barometer correction have not been applied. The storm surge height SS is obtained by correcting the altimeter TWLE for the global ocean tide model GOT4.8 [*Ray et al.*, 2011], which is among the highest quality tide models available today for shallow water region [*Stammer et al.*, 2014].

The in situ network, maintained by the Water and Shipping Administration (WSV) and by the DWD (Deutscher Wetterdienst), consists of thirteen stations providing both continuous GPS measurements (CGPS) and water level data, four stations with U10 data (FINO1, FINO3, Borkum, Norderney) and six stations with SWH data (FINO1, FINO3, Helgoland, Elbe, Westerland and Lighthouse Alter Weser) (Figure 1). The sampling is one minute for water level, 10 min for U10 and 30 or 60 min for SWH data. GPS data are recorded every 30 s, while results are derived with a 1 min sampling rate.

We subtract the ocean tide computed by the Matlab software T_TIDE [*Pawlowicz et al*., 2002] from the tide gauge readings to obtain the storm surge height at the tide gauge stations.

Two model simulations of water heights are considered to predict the surge. The first surge is derived from model BSHcmod [*Dick et al*., 2001] corrected for the tide-only run of the same model. BSHcmod is the regional operational numerical circulation model of the German Federal Maritime and Hydrographic Agency (BSH) and is driven by the meteorological models GME and COSMO-EU of the German weather service (DWD). This surge is called DWD/BSH hereafter.

The second surge simulation is the JRC Storm Surge Calculation System, named Hyflux2 [*Probst and Franchello*, 2012], which uses meteorological forecasts produced by the European Centre for Medium-Range Weather Forecasts (ECMWF). This surge is called ECMWF/JRC hereafter.

The predicted wind speed is from COSMO-EU/DWD (hereafter DWD) and ECMWF. The predicted wave height is from the Local Wave Model (LSM, hereafter DWD/BSH), driven by the DWD winds [*Behrens and Schrader*, 1994], and from the ECMWF Interim Reanalysis model (ERA-Interim). Finally 6-hourly surface pressure and wind speed data are from the NOAA/NCEP Global Forecast System (NOAA/GFS) model and from ERA-Interim. See Table S1 in the supporting information for model parameters and resolution.

For the validation of SS, SWH, and U10 we use the mean, standard deviation (STD), and root mean square (RMS) of the difference between model and observation, correlation (cor) between both, slope of the regression line through the origin, and scatter index defined as the standard deviation of the data with respect to the best fit line divided by the mean value [*von Storch and Zwiers*, 1999].

2.2. Vertical Displacement

The nontidal vertical displacements estimated from GPS observations and predicted by the model simulations are compared. For the GPS analysis, we consider the 13 CGPS receivers at tide gauges and additional 37 International GPS Service sites in Northern Europe are added for datum definition and regional coverage. The input data rate is 30 s and the elevation cutoff angle is set to 5°. Data have been processed using the Bernese GPS Software Version 5.2 [*Dach et al*., 2007]. Solid earth and pole tides are modeled according to the International Earth Rotation Service Conventions. For 2-hourly troposphere estimation, wet and dry Global Mapping Functions [*Boehm et al*., 2006] with a once per day gradient estimation according to *Chen and Herring* [1997] are applied. The GOT4.8 model is used to correct for the ocean tidal loading. Coordinates are computed in the ITRF2008 reference frame; kinematic positions are estimated at 1 min interval between 28 November and 15 December 2013. The changes in the vertical component of the CGPS at tide gauges are evaluated in three steps. First, outliers in the GPS estimates are eliminated by comparison of raw and smoothed time series by a 1 h moving average filter. Points with residual differences higher than 3 times the standard deviation are eliminated. The gaps in the cleaned time series are filled in by a linear interpolation. In the second step, a sidereal filter (SF) is applied, which consists of averaging the time series over several consecutive sidereal days to eliminate the periodical signals related to the configuration of the GPS satellites constellation [*Bock et al*., 2000]. The two days of the storm are neglected by creating the filter. Finally, a 6 h moving average is applied. The output is kept both at 1 and at 60 min sampling to match the surge model sampling. Noisy time series at five sites (TGEM, TGWH, HOE2, TGCU, and TGDA) are not considered further. We evaluate the Earth's response to the loading [*Farrell*, 1972] predicted by the storm surge models using the program SPOTL [*Agnew*, 1997]. As we analyze the transient and relative effects of the storm surge in a regional approach no corrections for center of figure and center of mass differences in predicted and observed deformations are made, see *Geng et al*. [2012].

3. Results

3.1. Along-Track and Cross-Shelf Surge Variations

The ascending pass 629 of the SARAL mission crosses the North Sea at 4:47 UTC on 6 December. The tide gauge in Helgoland is 20 km from the SARAL ground track (Figure 1). Its data indicate a maximum storm surge SS of 2.95 m at the time of the SARAL/AltiKa overflight. The maximum SS occurred at low tide and the maximum sea level (3.57 m) was recorded during high tide, 4 h before (Figure 2, top). At the FINO1 platform, 30 km away from SARAL ground track, the buoy recorded SWH higher than 8 m for many hours including the time of the SARAL overflight. In FINO1 and in Borkum (TGBF) the wind speed remained close

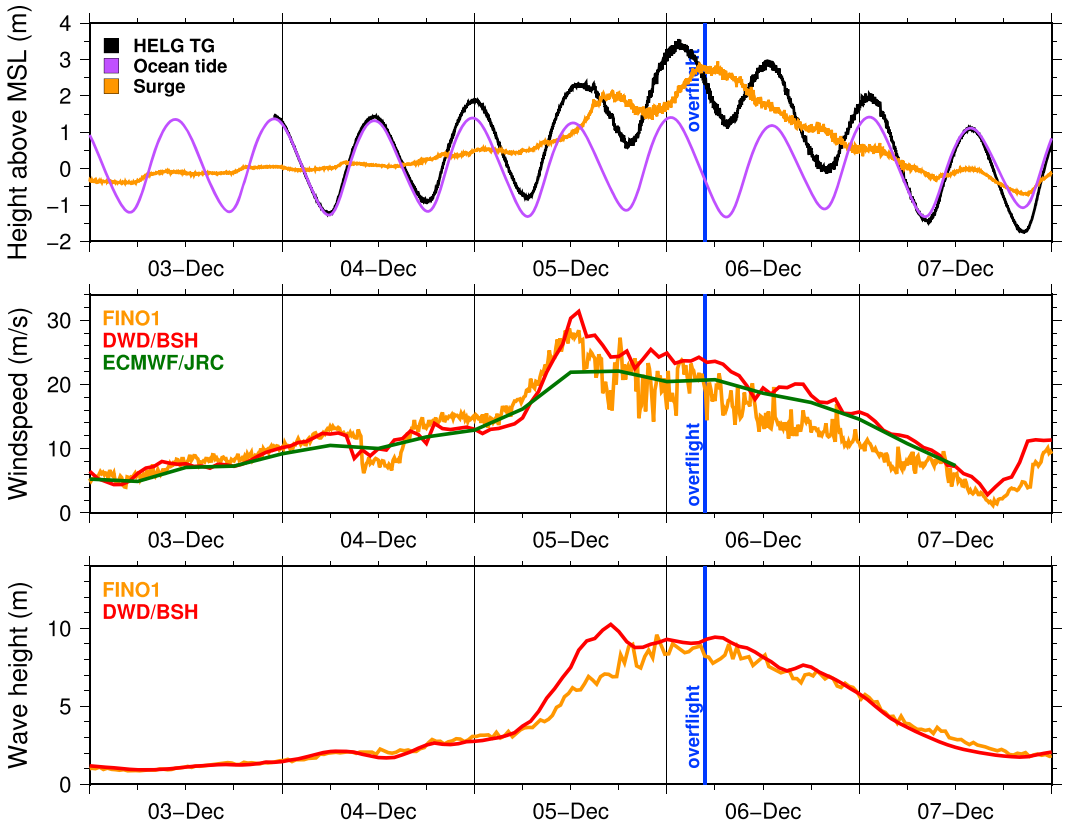

Figure 2. Observed water level and estimated ocean tide with (top) derived surge at Helgoland tide gauge, (middle) observed and simulated wind speed and (bottom) wave height in FINO1. Time of the SARAL overflight is indicated.

to 22 m/s for many hours and was still about 20 m/s at the time of the SARAL overflight (Figure 2). The maximum wind speed of 23 m/s preceded the maximum height of the storm surge by half a day. At the same time, at most of the coastal stations, the measured waves were, instead, lower than 7 m. Part of the difference is likely due to the location of the instruments, as some anemometers are located on land, while the ones at TGBF and FINO1 are in open water. The satellite-derived SS, SWH, and U10 are significantly different from values measured in cycles before and after the storm (see light and dark gray lines in Figure 3, right).

The SS at the along-track location closest to the coast (B1, 8 km away from the Langeoog island, see Figure 1, right) was 2.83 m high. Considering the distance of 25 km between Helgoland and the nearest point along track (B2), the difference of 0.1 m between the altimetry and the tide gauge values is small. The surge is still noticeable along track up to 400 km into the North Sea, resulting in a large offshore slope. The altimeter-derived SS and the SS predicted by model simulations agree in time with some discrepancies in magnitude. In general, the DWD/BSH model overestimates the SS height, while the JRC model underestimates it. The RMS of their differences is around 0.3 m, with mean near to zero. The HyFlux2 simulation forced by the DWD COSMO-EU wind field, the predicted surge (hereafter DWD/JRC) has the best agreement with the altimetric surge (STD is 0.2 m, Table S3). Another reason for discrepancies between the surge models could be the model resolution, as precise bathymetry is needed to capture small-scale effects in the Wadden Sea [*Arns et al.*, 2013].

Figure 3 (left) shows the snapshot of the three models at the time of the overflight; the surge derived from the tide gauges is also drawn. Altimetry observes extreme values also for wave height and wind speed. The wind speed of about 18 m/s exceeds all winds measured by altimetry during the previous 9 months, which are always lower than 10 m/s. The highest U10 is predicted by COSMO-EU and reaches 25 m/s, the lowest U10 is obtained using ERA-Interim and ECMWF. The RMS of the U10 differences is around 3–4 m/s, with mean and STD of 4 m/s and 0.6 m/s, respectively. More strikingly, the altimeter-derived SWH of up to 13 m is much higher than the 5 m maximum recorded in the previous year. The SWHs from wave model LSM are higher

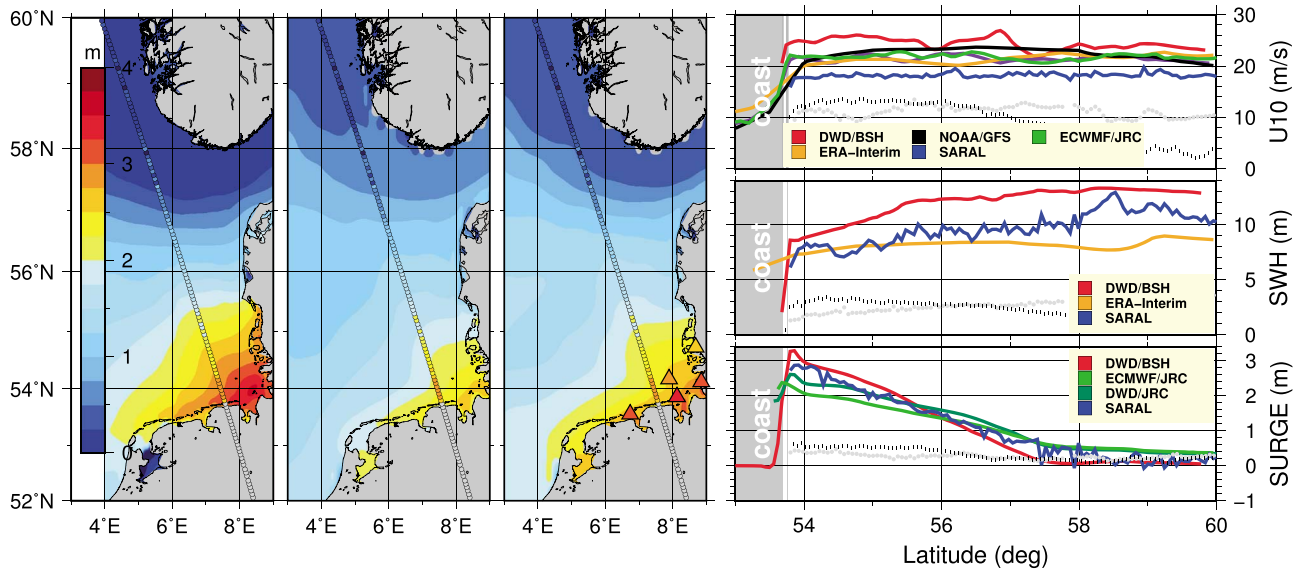

Figure 3. (left) Surge at the time of the overflight predicted by BSHcmod and HyFlux2 simulations with various wind forcing (DWD/BSH, ECMWF/JRC and DWD/JRC from left to right) and derived from in situ data (triangle). (right) Profiles at the SARAL/AltiKa overflight of wind speed, significant wave height, and surge height derived from altimeter observations (blue) and from models (red for DWD/BSH, light green for ECMWF/JRC, dark green for DWD/JRC, orange for ERA-INTERIM, and black for NOAA/GFS). Gray lines correspond to observations before (continuous line) and after Cyclone Xaver (black points).

than the altimeter-derived SWH, while those from ERA-Interim are lower. The RMS of the differences between observed and predicted values from the first simulation is around 2.5 m, with mean and STD of 2.3 m and 0.8 m, respectively (Table 1). We note that the altimeter-derived wind speed values are lower than all wind model data considered; this may be due to an overestimation of the atmospheric attenuation of the radar power. Indeed, a dedicated algorithm based on the radiometer measurements was developed to adjust the measured power for this attenuation. The correction in the products is larger than the attenuation determined based on surface pressure, near-surface temperature, and water vapor content [*Lillibridge et al*., 2014], the larger attenuation correction would result in a too large estimation of backscatter and hence in a reduced wind speed.

Comparison of models with the offshore in situ data over the 5 days around the event confirms the results found with the altimeter comparison. In Helgoland the STD is 0.2 m for SS height, 0.7 m for SWH, and 2.2 m/s for U10 (Table 1); the largest differences are at peak event.

Table 1. Empirical Standard Deviation S_N (mm), S_N Reduction (%) Obtained by Correcting the Estimation for the Prediction, Correlation Between Hourly Estimated (GPS) and Predicted Vertical Displacement[a]

	BORJ	TGBF	HELG	TGME	LHAW	FLDW	TGBH	TGBU
GPS S_N	9.4	8.6	9.1	9.1	10.7	9.4	5.2	7.5
ECMWF/JRC S_N	9.6	9.4	9.5	8.4	8.7	7.8	5.3	6.5
GPS-ECMWF/JRC S_N	4.8	4.5	3.6	3.4	6.2	4.3	2.9	5.9
S_N Reduction (%)	49	47	61	63	42	54	**44**	21
Corr GPS&ECMWF/JRC	87	88	93	93	81	89	**85**	**65**
DWD/JRC S_N	8.4	8.2	8.6	7.6	8.0	7.1	4.8	6.1
GPS-DWD/JRC S_N	4.2	3.6	3.6	2.9	5.6	3.9	2.9	5.8
S_N Reduction (%)	**55**	**58**	**61**	**68**	**47**	**59**	**44**	**22**
Corr GPS and DWD/JRC	**89**	**91**	92	**96**	**86**	**93**	84	65
DWD/BSH S_N	10.9	10.7	11.7	10.3	10.8	9.6	6.2	7.9
GPS-DWD/BSH S_N	5.2	5.2	4.1	4.3	7.2	5.2	3.8	6.5
S_N Reduction (%)	45	40	54	53	32	45	27	13
Corr GPS and DWD/BSH	88	88	**95**	91	77	85	80	64

[a]Interval is 5–6 December 2013. Bold values indicate the highest values for a given station.

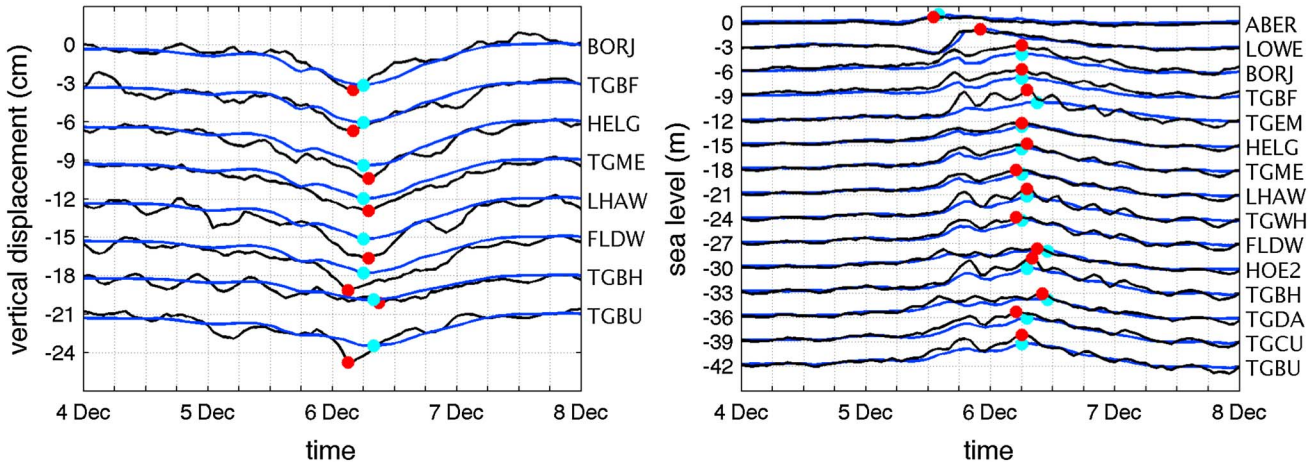

Figure 4. (left) Vertical loading displacement estimated at the eight GPS stations (black) and predicted by the HyFlux2 DWD/JRC model (blue). (right) Storm surge height estimated at 15 tide gauges (black) and predicted by the same model (blue). Sampling is 1 h, time interval is 5–6 December 2013. The vertical spacing between time series is set to 3 cm and 3 m, respectively. Markers show maxima for both estimated (red) and predicted (light blue) values.

3.2. Land Subsidence and Alongshore Surge Variation

To assess the error in the vertical GPS displacement, we calculate its empirical standard deviation (S_N) over 1 week not influenced by the storm, for both 1 and 60 min data. The S_N ranges between 3.7 and 6.2 mm, for all but one station (TGBH) and is within the limits for vertical subdaily kinematic GPS solution of about 7 mm [*Bock et al.*, 2004].

The down sampled 1 h GPS vertical displacements are compared to the vertical storm surge loading deformation derived from the lowest time resolution model. The estimates are corrected for the prediction, and the best model is chosen according to the highest reduction in S_N and highest correlation between observed and predicted subsidence. The DWD/JRC model performs best for all the stations according to the S_N reduction criteria and for most of them according to the correlation (Table 1). All in all, estimation and prediction are in excellent agreement, with a standard deviation of the differences smaller than 5.8 mm at all the stations. Figure 4 (left) shows the subsidence observed by GPS and predicted by the DWD/JRC model. The maximum subsidence (red/blue dots) follows the anticlockwise path of the storm (see Table S4 for 1 min GPS values). The vertical displacement reaches 3–5 cm at most stations. It occurs first at the western (BORJ and TGBF) and later at the eastern (TGBH) stations. Exceptions are FLDW and TGBU, probably for bathymetry effects.

Similarly to the subsidence, we analyze the differences between observed and predicted surge. Model DWD/JRC performs best again (Table S5 and Figure 4 (right), see time and maximum subsidence in Table S6). The surge height reaches values between 2.5 and 4.3 m in the German Bight and has two maxima, the first on 5 December, the second, the day after. The Aberdeen and Lowerstoft stations in the UK, located 550 km apart, have only one maximum 8 h apart. This indicates a shelf wave propagating anticlockwise along the coasts of the North Sea with a speed of about 60 km/h. This wave reached the eastern coast of the North Sea about 10 h after its arrival in Lowerstoft; it caused the second SS maximum observed at all the German stations. Instead, the first maximum is caused by wind forcing and appears in TGDA and HOE2 at the same time of the shelf wave in Aberdeen (see Figure 4, right). Observed and predicted time and magnitude of the second SS maximum agree (Table S6). Both surge components merge at the second maximum producing the extreme surge described above, see Movie S1, which represents DWD/BSH simulated surge height and vertical displacement.

4. Conclusions

For the first time a storm surge event at its maximum has been analyzed in an integrated approach of in situ altimetry and GPS satellite geodetic data and models. The altimeter satellite SARAL took a unique snapshot of the Xaver storm surge in the German Bight in December 2013 observing sea level, wind, and wave height along a pass. Thus, the altimeter could display the shape of the storm surge as a function of the distance to

the coast in a geodetic reference frame. In situ data were considered as well to gain alongshore information and to detect storm surge vertical deformations. The main goal was to monitor the storm surge spatial evolution and to identify which information is given by each observing component. The second main goal was to detect errors and deficiencies in both observations and models.

First, we have considered each observation type. Indeed, all observations are required for a complete description of the evolution of the surge height, due to both a direct, large-scale forcing and a shelf wave dynamics with anticlockwise propagation. While the in situ tide gauge network monitors the propagation of the surge, geometric deformation appears to be more affected by the shelf wave dynamics than by large-scale forcing. Satellite altimetry provides an instantaneous snapshot of the complex reality, unique for its spatial information. Finally, both evolutions are correctly represented in the regional predictions by all models.

We have also analyzed differences between different observing systems and between observed and predicted values. We have shown that differences between altimeter observations and predictions are comparable to differences between model predictions. The models vastly differ, for example, on wind field, with values lower in ECMWF than in DWD. We then found that surge heights are overestimated in the DWD/BSH and underestimated in the ECMWF/JRC simulation. Similarly, DWD and the ECMWF winds, respectively, overestimated (by about 5 m/s) and underestimated (by up to 10 m/s) the altimeter-derived wind. Comparisons between model and in situ data show similar results suggesting that the largest differences between data and models occur at the time of the extreme event.

We could show that the difference in surge heights between the two simulations arises from the lower wind forcing in ECMWF/JRC. In fact, when Hyflux2 is initialized with DWD pressure/wind forcing, the predicted DWD/JRC surge heights are closer to the DWD/BSH model.

One relevant result of our study is the detection of a surge-induced vertical land movement, of 3–5 cm at the maximum, of the surge at seven out of eight stations of the network, in good agreement with the loading predicted for the DWD/JRC surge. This confirms the potential of the GPS network to monitor the storm surge spatial evolution in near-real time by a suitably distributed network of coastal GPS sites. Temporal and spatial evolution of the vertical displacement observed by GPS are more affected by shelf wave dynamics than by direct local wind forcing. Indeed both components are simulated in regional predictions, and their accuracy can be improved by using the available geodetic data.

Finally, we have shown that the altimeter observations reproduce the surge amplitude within a few centimeters all along-track offshore up to a few kilometers to the coast, also during extreme events. Therefore, assimilation of altimeter-derived heights in operational storm surge and circulation models appears promising to reduce offshore uncertainties in the storm surge prediction. The results strongly depend on the spatial availability of the altimeter data, and consequently, several satellites are necessary. On the other hand, improvements are also needed in altimeter data processing since SARAL/AltiKa products underestimate extreme wave height by 2–3 m and wind speed by 5–10 m/s.

Acknowledgments

The authors acknowledge, for in situ and model data, the Bundesanstalt für Gewässerkunde (BfG), the German Federal Agency for Cartography and Geodesy (BKG), the Bundesumweltministerium (BMU), Project Management Jülich (PTJ), the WSV, BSH, DWD, and ECMWF. The free available software programs SPOTL and T-tide were used. We thank Sönke Dangendorf and two anonymous reviewers for their suggestions which improved the manuscript. Support of the Deutsche Forschungsgemeinschaft (DFG) through project 'Coastal Sea Level' (COSELE) and of the ESA Climate Change Initiative (CCI) is kindly acknowledged.

References

Agnew, D. C. (1997), NLOADF: A program for computing ocean tide loading, *J. Geophys. Res.*, *102*(B3), 5109–5110, doi:10.1029/96JB03458.

Andersen, O. B., and P. Knudsen (2010), The DTU10 mean sea surface and mean dynamic topography: Improvements in the Arctic and coastal zone, Ocean Science Topography Science Team Meeting, Lisbon, Portugal, 19–21 Oct.

Arns, A., T. Wahl, S. Dangendorf, C. Mudersbach, and J. Jensen (2013), Ermittlung regionalisierter Extremwasserstände für die Schleswig-Holsteinische Nordseeküste, *Hydrol. Wasserbewirtsch.*, *57*, 264–278.

Behrens, A., and D. Schrader (1994), The wave forecast system of the Deutscher Wetterdienst and the Bundesamt für Seeschifffahrt und Hydrographie: A verification using ERS-1 altimeter and scatterometerdata, *Dtsch. Hydrogr. Z.*, *46*(2), 131–149, doi:10.1007/BF02225836.

Bock, Y., R. M. Nikolaidis, P. J. de Jonge, and M. Bevis (2000), Instantaneous geodetic positioning at medium distances with the Global Positioning System, *J. Geophys. Res.*, *105*(B12), 28,223–28,253, doi:10.1029/2000JB900268.

Bock, Y., L. Prawirodirdjo, and T. I. Melbourne (2004), Detection of arbitrarily large dynamic ground motions with a dense high-rate GPS network, *Geophys. Res. Lett.*, *31*, L06604, doi:10.1029/2003GL019150.

Boehm, J., B. Werl, and H. Schuh (2006), Troposphere mapping functions for GPS and very long baseline interferometry from European Centre for Medium-Range Weather Forecasts operational analysis data, *J. Geophys. Res.*, *111*, B02406, doi:10.1029/2005JB003629.

Chen, G., and T. Herring (1997), Effects of atmospheric azimuthal asymmetry on the analysis of space geodetic data, *J. Geophys. Res.*, *102*(B9), 20,489–20,502, doi:10.1029/97JB01739.

Dach, R., U. Hugentobler, P. Fridez, and M. Meindl (2007), Bernese GPS Software Version 5.0, User manual, Astronomical Institute, Univ. of Bern., Astronomical Institute, Univ. of Bern.

Dangendorf, S., S. Mueller-Navarra, J. Jensen, F. Schenk, T. Wahl, and R. Weisse (2014), North Sea storminess from a novel storm surge record since ad 1843, *J. Clim.*, *27*, 3582–3595, doi:10.1175/JCLI-D-13-00427.1.

Dick, S., E. Kleine, S. H. Müller-Navarra, H. Klein, and H. Komo (2001), The operational circulation model of BSH (BSHcmod), Berichte des Bundesamtes für Seeschifffahrt und Hydrographie, N. 29/2001.
Farrell, W. E. (1972), Deformation of the Earth by surface loads, *Rev. Geophys.*, *10*, 761–797, doi:10.1029/RG010i003p00761.
Geng, J., S. D. P. Williams, F. N. Teferle, and A. H. Dodson (2012), Detecting storm surge loading deformations around the southern North Sea using subdaily GPS, *Geophys. J. Int.*, *191*(2), 569–578.
Han, G., Z. Ma, D. Chen, B. de Young, and N. Chen (2012), Observing storm surges from space: Hurricane Igor off Newfoundland, *Sci. Rep.*, *2*, 1010, doi:10.1038/srep01010.
Jensen, J., and S. H. Mueller-Navarra (2008), Storm surges on the German Coast, *Die Küste*, *74*, 92–124.
Lillibridge, J. L., M. Lin, and C. K. Shum (2013), Hurricane Sandy storm surge measured by satellite altimetry, *Oceanography*, *26*(2), 8–9, doi:10.5670/oceanog.2013.18.
Lillibridge, J. L., R. Scharroo, S. Abdalla, and D. C. Vandemark (2014), One- and two-dimensional wind speed models for Ka-band altimetry, *J. Atmos. Oceanic Technol.*, *31*(3), 630–638, doi:10.1175/JTECH-D-13-00167.1.
Mathers, E. L., and P. L. Woodworth (2004), A study of departures from the inverse-barometer response of sea level to air-pressure forcing at a period of 5 days, *Q. J. R. Meteorol. Soc.*, *130*, 725–738, doi:10.1256/qj.03.46.
Pawlowicz, R., B. Beardsley, and S. Lentz (2002), Classical tidal harmonic analysis including error estimates in MATLAB using T-TIDE, *Comput. Geosci.*, *28*(8), 929–937, doi:10.1016/S0098-3004(02)00013-4.
Probst, P., and G. Franchello (2012), Global storm surge forecast and inundation modeling, EUR 25233, Joint Research Centre, European Commission.
Ray, R. D., G. D. Egbert, and S. Y. Erofeeva (2011), Tide predictions in shelf and coastal waters: Status and prospects, in *Coastal Altimetry*, edited by S. Vignudelli et al., Springer, Berlin.
Rossiter, J. R. (1958), Storm surges in the North Sea, 11 to 30 December 1954, *Philos. Trans. R. Soc. London*, *251*(991), 139–160, doi:10.1098/rsta.1958.0012.
Scharroo, R., W. H. F. Smith, and J. L. Lillibridge (2005), Satellite altimetry and the intensification of Hurricane Katrina, *Eos Trans. AGU*, *86*(40), 366, doi:10.1029/2005EO400004.
Scharroo, R., E. W. Leuliette, J. L. Lillibridge, D. Byrne, M. C. Naeije, and G. T. Mitchum (2013), RADS: Consistent multi-mission products, Proceedings of the Symposium on 20 Years of Progress in Radar Altimetry, Spec. Publ., ESA SP-710
Stammer, D., et al. (2014), Accuracy assessment of global barotropic ocean tide models, *Rev. Geophys.*, *52*, 243–282, doi:10.1002/2014RG000450.
von Storch, H., and F. Zwiers (1999), *Statistical Analysis in Climate Research*, Cambridge Univ. Press, Cambridge, U. K.
Weisse, R., and H. von Storch (2009), *Marine Climate and Climate Change: Storms, Wind Waves and Storm Surges*, Springer, Heidelberg, Germany.
Weisse, R., H. von Storch, H. D. Niemayer, and H. Knaack (2012), Changing North Sea storm surge climate: an increasing hazard?, *Ocean Coast. Manag.*, *68*, 58–68.
Williams, S. D. P., and N. T. Penna (2011), Non-tidal ocean loading effects on geodetic GPS heights, *Geophys. Res. Lett.*, *38*, L09314, doi:10.1029/2011GL046940.
Zerbini, S., F. Matonti, F. Raicich, B. Richter, and T. van Dam (2004), Observing and assessing nontidal ocean, continuous GPS and gravity data in the Adriatic area, *Geophys. Res. Lett.*, *31*, L23609, doi:10.1029/2004GL021185.